Cluster formation in symmetric binary SALR mixtures

Cluster formation in symmetric binary SALR mixtures

Jiazheng Tan, N. D. Afify, Carlos A. Ferreiro-Rangel, Xianfeng Fan, and M. B. Sweatman[a)]
School of Engineering, The University of Edinburgh, The King's Buildings, Sanderson Building, Mayfield Road, Edinburgh EH9 3JL, United Kingdom

(Dated: 25 January 2021)

The equilibrium cluster fluid state of a symmetric binary mixture of particles interacting through short-ranged attractive (SA) and long-ranged repulsive (LR) interactions is investigated through Monte Carlo simulations. We find the clustering behavior for this system is controlled by the cross-interaction between the two types of particles. For a weak cross-attraction, the system displays behavior that is a composite of the behavior of the individual components, i.e. the two components can both form giant clusters independently and the clusters distribute evenly in the system. For a strong cross-attraction, we instead find the resulting clusters are mixtures of both components. Between these limits, both components can form relatively pure clusters, but unlike clusters can join at their surfaces to form composite clusters. These insights should help to understand the mechanisms for clustering in experimental binary mixture systems, and help tailor the properties of novel nanomaterials.

I. INTRODUCTION

Clusters exist widely in science and nature, for example in protein solutions[1], biomineralisation[2], crystal formation[3,4], nano material manufacturing[2,5,6] ring polymers[7,8] and self-propelled particles[9,10]. A typical case investigated by Ramdzan and collaborators[11] shows that the clustering behavior of protein molecules influences their structure and function and is associated with neurodegenerative diseases. Alternatively, the self-assembly of giant clusters in solution is thought to be the first step in the templating of certain nanomaterials[12]. And, Truskett[13,14] propose the use of clusters to design porous materials with well-defined voids.

Generally speaking, there are two types of clustering system, equilibrium and non-equilibrium. For non-equilibrium clusters, arrested networks[15,16] and gels[17,18] are two kinds of typical examples and a good introduction to this body of work is provided by Zaccarelli et al.[19,20].

The focus of this paper, however, is on systems that exhibit uniformly dispersed giant equilibrium clusters, also known as the cluster fluid state. Such clusters are known to form in SALR fluids at low concentrations, where particles interact through short-range attractive and long-range repulsive interactions[21]. 'Giant' clusters are separated from ordinary clusters involving just a few particles by a minimum in the concentration, and therefore a maximum in the formation free energy, of intermediate-sized clusters.

This physics is very general and can apply at any length scale, from nucleons thorough to, in principle, large 'agents' such as humans[22]. However, the phenomenon of giant equilibrium clustering seems to be especially prominent and important in molecular and cell biology. It is tempting, therefore, to try to understand the formation of giant clusters in many diverse systems, but especially those in biological systems, in terms of the physics of SALR fluids.

However, many biological systems in which clusters are observed involve more than one kind of component. For example, Sweatman and Insall[23] study a model binary SALR mixture designed to replicate the behavior of a specific kind of membraneless organelle formed from two specific proteins. Therefore, it is important to understand at a fundamental level the additional complexity these binary SALR mixtures offer beyond the single component case.

Regarding the single-component equilibrium cluster fluid, Sweatman et al.[21] studied the clustering behavior of pure component SALR fluids at low concentrations through a novel kind of coarse-grained density functional theory, that is essentially an extended type of micelle theory, as well as Monte Carlo simulation, finding a novel cluster vapour to condensed cluster phase transition[24]. Furthermore, Sweatman[25] reports that these clusters can reproduce, or fission, when the system concentration increases sufficiently slowly. Earlier work by Archer and Wilding involving more familiar types of density functional theory[26] and/or Monte Carlo simulation[27] revealed a hierarchy of clustering transitions as the system concentration increases, that take the system from a condensed cluster phase to the bulk liquid.

Several works have investigated the onset of clustering in pure component SALR fluids in an attempt to define when clustering occurs. For example, using Monte Carlo simulation, Godfrin et al.[28] provide an empirical criteria for discrimination between a homogeneous solution and a genuine clustered state based on the magnitude of the low-q peak in the structure factor. The result of Godfrin et al.[28] has been explored further by Bomont and colleagues[29] using Monte Carlo simulation, which further reveal the relationship between the criteria and the local density of the fluid. Also, Truskett[30] provided a refinement, which suggests that a comprehensive consideration of both the height and the width of this peak can make more precise judgements.

Ordered, or modulated, cluster states at concentrations above that of the disordered cluster fluid can be modeled using standard mean-field density functional approaches[31,32]. For example, Archer and colleagues[31] further extend previous results[27] by developing a theory for the phase transition from the uniform fluid to a striped phase. However, this work ignores the intervening cluster fluid phase. Indeed, it is in principle impossible for such approaches to treat the kinds of cluster fluid phase of interest to us.

Integral equation approaches might be able to treat the clus-

[a)]Electronic mail: martin.sweatman@ed.ac.uk

ter fluid phase if suitable bridge functions can be found. For example, the earlier result of Bomont and colleagues[29] was extended based on integral equation theory[33,34], supporting conclusions from simulations. Also, using a thermodynamically self-consistent integral equation theory, Bomont and colleagues[35] find jumps in the first peak of the radial distribution function for a range of SALR parameters, indicative of a potential phase transition from a uniform phase to a modulated clustered phase at intermediate densities. Despite the significant advance it brings, no results are provided at low density for the cluster fluid state. Indeed, it remains the case that while integral equation approaches can reveal the onset of clustering behavior in a uniform fluid, they are presently unable to quantitatively capture the structure and thermodynamics of the cluster fluid state. The main reason for this is that their bridge functions are typically designed for mathematical convenience, and lack the physical insight required.

In summary, while good progress has been made with understanding pure component SALR fluids generally, the cluster fluid phase specifically has proven more difficult to treat, with analysis typically limited to simulation work or the coarse-grained approach of Sweatman and colleagues[21]. Moreover, all this earlier work is focused on one-component systems. Regarding mixtures, Ferreiro-Rangel and Sweatman[36] extended the results of Sweatman et al.[21] to systems with binary mixtures of SALR/SA particles, showing that the clusters are typically composed of a more equal mixture of SA and SALR particles for a strong cross-interaction. And Sweatman and Insall[23] investigated an SALR mixture as a model for protein complexes adsorbed at cell membranes. To the best of our knowledge, however, a fundamental understanding of the binary SALR mixture case remains open.

Here, as an initial step in this direction, we focus for simplicity on the symmetric case where A-A and B-B interactions are identical, but A-B interactions are different. Non-symmetric cases will be studied in future work. The main motivation of the symmetry assumption is to reduce the degrees of freedom so that the problem is more amenable to study. However, we expect the results in this paper will also apply to practical mixtures where the two components are very similar, but not necessarily perfectly symmetric. The focus, therefore, of this paper is to reveal, using Monte Carlo simulations, the effect of different A-B cross interactions on clustering behavior of the mixture. As for Sweatman et al.[21], we focus in this initial work on the low density region of the phase diagram where uniformly dispersed spherical clusters are expected to occur. As for the single component case[27], higher concentrations are expected to lead to a hierarchy of clustering transitions among modulated structures. Again, we emphasize our interest on equilibrium fluids, which can also provide insights to the behavior of non-equilibrium or frustrated systems, such as gels and glasses.

The organization of this paper is as follows. In Section II, computational details of the Monte Carlo simulations, as well as the model parameters, are given. Simulation results and analysis are presented in section III. Finally, a summary of this work with some potential future directions is provided in Section IV.

II. COMPUTATIONAL DETAILS

This work focuses on fluids consisting of binary mixtures of components A and B, with particles from both components interacting through short range attractive and long range repulsive (SALR) forces. Following Sweatman et al.[21], these SALR interactions are modelled by double-Yukawa potentials, extended here to the mixture case. Therefore, hard sphere interactions occur for $r < d$, while for $r > d$,

$$\begin{aligned} \phi_{DYij}(r) &= -\phi_{SAij}(r) + \phi_{LRij}(r) \\ \phi_{SAij}(r) &= \frac{A_{aij}}{r} exp[-z_{aij}(r-1))] \\ \phi_{LRij}(r) &= \frac{A_{rij}}{r} exp[-z_{rij}(r-1))] \end{aligned} \tag{1}$$

Here, the term ϕ_{SAij} represent the short-range attraction, the term ϕ_{LRij} represent the long-range repulsion and $i, j = A, B$. The parameters A_{aij} and A_{rij} represent the magnitude of the attractive and repulsive interaction respectively, while the parameters z_{aij} and z_{rij} represent the inverse decay length of the attractive and repulsive interaction respectively.

Sweatman et al.[21] showed that giant clusters occur at low system concentrations for the pure SALR fluid with the following parameters; $A_a \in [1.6, 2.2]$, $A_r = 0.5$, $z_a = 1$,$z_r = 0.5$ and an overall system density approximately in the range $\rho_b \in [0.01, 0.1]$ (note that reduced units are used throughout this work, so that energies are given in units of k_BT, with k_B being Boltzmann's constant and T being the temperature, lengths are stated relative to the hard sphere diameter, d, and density is given in units of particles per d^3). Based on their work, to ensure both components of our symmetric binary SALR fluid by themselves would also exhibit clustering we choose the direct interaction parameters $A_{aAA} = A_{aBB} = 1.75$, $A_{rAA} = A_{rBB} = 0.5$, $z_{aAA} = z_{aBB} = 1$, and $z_{rAA} = z_{rBB} = 0.5$ where each component has an overall system density of 0.024. Many other choices are, of course, possible since the space in which giant clusters appear for this type of pair interaction is large and high dimensional. The values used by Sweatman et al.[21] were chosen to avoid problems with 'sticky' particles, i.e. strong short-ranged interactions, which would inevitably lead to sampling problems in simulations, and are similar to those used by others[27].

As our aim is to investigate the effect of the cross-interaction parameters on clustering, for consistency with the direct interactions and to avoid problems with sampling in the simulations, we choose, $A_{aAB} = 0.35, 0.7, 1.05$ and $A_{rAB} = 0.1, 0.2, 0.3$, while also choosing $z_{aAB} = 1$ and $z_{rAB} = 0.5$. We therefore study nine different combinations of the cross-interaction strength, and observe its effect on clustering behavior. We expect these parameter ranges cover the fundamental behavior of interest to us, and this is borne out by the results. There is, therefore, no need to provide a more extensive search of parameter space. In this paper, for all the simulations, the cut-off is equal to the half of the box side. Con-

sequently, for direct and cross-interactions, the largest step at cut-off is smaller than 2×10^{-7}.

Because we are interested in the equilibrium properties of these SALR fluids, we use the same canonical ensemble Monte Carlo methods as in earlier work[21]. Briefly, we use two different types of move; individual particle moves and cluster moves. For individual particle moves, to enable efficient sampling of low and high concentration regions, a dual Monte Carlo step size is employed with maximum step sizes of 0.5 and 10 respectively (chosen randomly with equal probability). Cluster moves are designed to efficiently equilibrate cluster degrees of freedom. First, a particle is chosen at random. Then, all particles within a sphere of radius 8 of this particle are moved by the same small vector with maximum length 2. To ensure microscopic reversibility, cluster moves are automatically rejected if the reverse move would involve a different group of particles. Molecular dynamics and Brownian dynamics simulations are other options for equilibrium simulations, although their sampling of cluster degrees of freedom might not be as efficient as our Monte Carlo scheme.

III. RESULTS AND DISCUSSION

We observe three kinds of general clustering behavior for these symmetric SALR fluids in Figure 1, called situation 1, 2 and 3. In situation 1, clusters consist mainly of component A or component B, and are uniformly distributed in the system. In situation 2, clusters consist mainly of component A or component B, but they combine, or 'stick' together, to form large composite clusters. In situation 3, mixed clusters consist of both component A and B and are uniformly distributed. Due to symmetry, these are all the expected possibilities for symmetric SALR fluids in the equilibrium cluster fluid state.

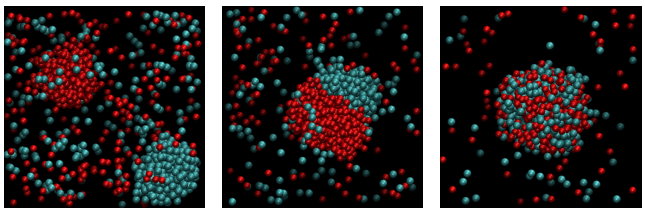

FIG. 1. Different general cluster situations, where red particles represent component A and blue particles represent component B.

While the pure and mixed clusters in situation 1 and 3 tend to be spherical, on average, the composite clusters in situation 2 are not. Instead, as they are formed from roughly spherical clusters that are stuck or squashed together, they tend to be elongated in one dimension. It is also the case that the mixed clusters in situation 3 can sometimes appear to contain domains enriched in one type of particle. However, no further structuring within mixed clusters is expected due to the symmetrical case we study, i.e. we do not expect to find core-shell structures or other asymmetric structures. The mixed clusters of situation 3 are easy to distinguish by eye from the clusters of situation 2. Further investigation of these different situations can be attempted though analysis of radial distribution functions, which is described later.

Figure 2 shows the energy plot of one representative case when $A_{aAB} = 0.7$ and $A_{rAB} = 0.2$. The three small snapshots represent different stages of this simulation. We see that the energy displays only small fluctuations around an identifiable mean after an initial equilibration stage. The longest fluctuations during this equilibration period likely reflect fluctuations in the largest degrees of freedom, the cluster positions.

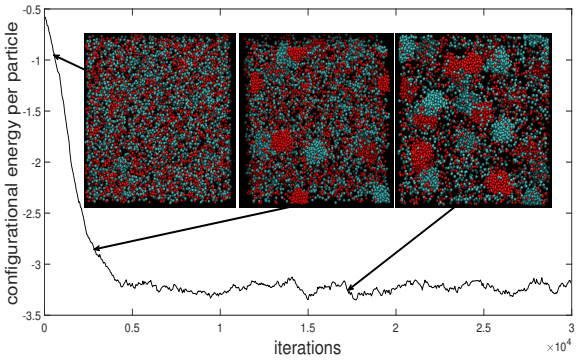

FIG. 2. Evolution of the configurational energy when $A_{aAB} = 0.7$ and $A_{rAB} = 0.2$. Each iteration consists of an attempt to move each particle individually and an attempted cluster move.

However, it is not clear whether the configuration depicted in Figure 2 is at equilibrium because once transitions in the number of giant clusters, i.e. cluster splitting or combining events, are unlikely to ever occur within a reasonable timescale. Essentially, these simulations cannot effectively sample fluctuations in the number of clusters, and therefore this simulation likely represents a metastable state.

However, as shown by Sweatman et al.[21] using their novel density functional theory developed specifically for these cluster fluid systems, the equilibrium state almost perfectly corresponds to the one with lowest configurational energy. This is because minima in the entropy density and the configurational energy density with respect to variation of the number of clusters almost exactly coincide. Therefore, to determine the equilibrium configuration one simply needs to repeat this simulation for different numbers of giant clusters, finding the one with the lowest configurational energy. The same approach is used in this work to identify the equilibrium configuration, except in one instance described in detail later. Simulations can be initiated with different numbers of giant clusters by selecting the output configuration of an initial simulation initiated with a random distribution of particles, which will tend to contain a large number of giant clusters, and successively redistributing, or 'killing', particles in the smallest remaining cluster. This will create a series of initial configurations, each with successively one fewer giant clusters. Average properties can be measured from the second half of the simulation.

The final snapshots of all nine simulations are shown in Figure 3. Each simulation consists of 4000 particles of each com-

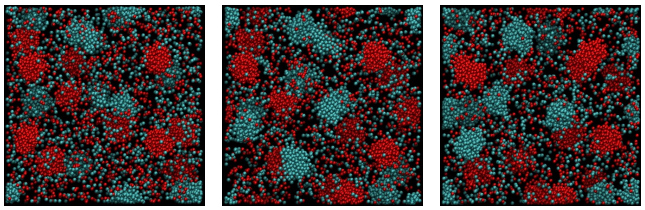

Case 1 $A_{aAB} = 0.35, A_{rAB} = 0.1$ | Case 2 $A_{aAB} = 0.35, A_{rAB} = 0.2$ | Case 3 $A_{aAB} = 0.35, A_{rAB} = 0.3$

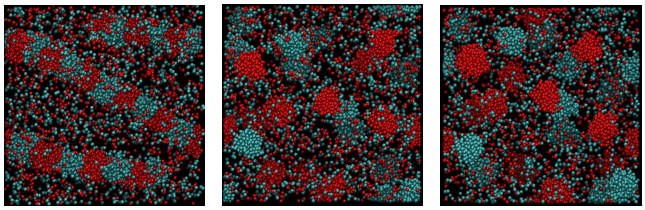

Case 4 $A_{aAB} = 0.7, A_{rAB} = 0.1$ | Case 5 $A_{aAB} = 0.7, A_{rAB} = 0.2$ | Case 6 $A_{aAB} = 0.7, A_{rAB} = 0.3$

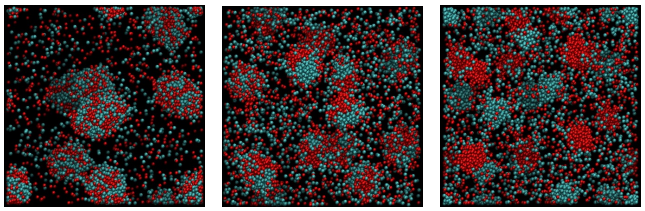

Case 7 $A_{aAB} = 1.05, A_{rAB} = 0.1$ | Case 8 $A_{aAB} = 1.05, A_{rAB} = 0.2$ | Case 9 $A_{aAB} = 1.05, A_{rAB} = 0.3$

FIG. 3. Final snapshots of nine simulations with different cross-interaction strengths. Each cubic simulation box is viewed along one of the main axes.

ponents and a cubic simulation box with period boundaries with side length 55, giving the required overall system density very close to 0.024 for each component. For each case, we used the method described above to find the equilibrium number and size of clusters, and Figure 3 shows snapshots from these equilibrium cases. Situation 1, consisting of a uniform dispersion of relatively pure clusters, is observed for cases 1, 2, 3, 5, 6, and 9. Situation 2 is observed in case 4, while situation 3 is observed in cases 7 and 8. In these latter two cases, although the clusters appear to contain domains enriched in one type of cluster, they are still easily distinguished from the clusters of case 4. To highlight this distinction, we consider their radial distribution functions in section III B. However, before that, further investigation is needed into case 4 to determine which basic situation it corresponds to. Case 7 produced the largest clusters, because it has the strongest attractive and weakest repulsive contributions to the cross-interaction.

A. Case 4

The final configuration for our initial simulation corresponding to case 4 consisted of several fused clusters, each of which was relatively pure. But this is unlikely to be the equilibrium situation because, although these simulations allow cluster moves, it remains very unlikely that, once formed, clusters will break up or merge during the limited simulation time available. Each simulation is, therefore, essentially sampling a metastable state. This is why, for each case, simulations with different numbers of clusters are performed to determine the equilibrium state, as described above. However, case 4 is a more difficult situation, as it requires different configurations of fused clusters to be simulated to determine the equilibrium. We therefore adopted the following strategy.

First, to find the correct number and size of individual clusters, we initiated simulations with specific numbers of clusters, just as for all the other cases studied. Comparison of the energy of each simulation, after an initial equilibration period, will reveal the expected equilibrium number and size of individual clusters. In a second step, we initiate simulations with different configurations of fused or composite clusters with a range of composite sizes, keeping the overall number of individual clusters at the equilibrium number (and therefore size) determined from the first step. Initial configurations are created by dragging individual particles within the VMD software[37]. Once again, comparison of the energy of these fused cluster configurations, after an initial equilibration period, will reveal which is the equilibrium configuration.

Figure 4 shows final configurations from the first step of this strategy. Each simulation consists of 3000 particles of each components and a cubic simulation box with period boundaries with side length 50, giving the required overall system density of 0.024 for each component. In each simulation, a pair of clusters, A and B, has merged to form a composite AB cluster of size 2 (in the following figures, the notation 'CC' is used to represent the concept 'composite cluster').

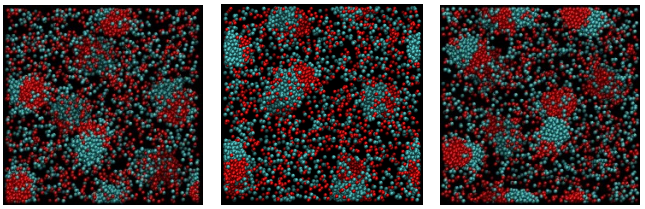

Number of cluster A: 8 Number of cluster B: 8 Number of CC: 8 | Number of cluster A: 9 Number of cluster B: 9 Number of CC: 9 | Number of cluster A: 10 Number of cluster B: 10 Number of CC: 10

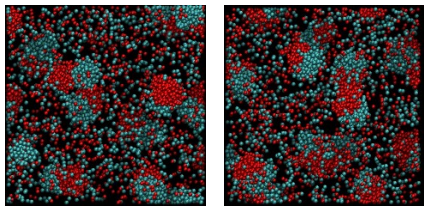

Number of cluster A: 11 Number of cluster B: 11 Number of CC: 11 | Number of cluster A: 12 Number of cluster B: 12 Number of CC: 12

FIG. 4. Final configurations for simulations initiated with different numbers of clusters when $A_{aAB} = 0.7, A_{rAB} = 0.1$.

The configurational energy for each configuration is shown in Figure 5. We therefore expect that the configuration with

11 clusters of each type is closest to equilibrium. However, as 12 is a more divisible number, we use this value in the next step.

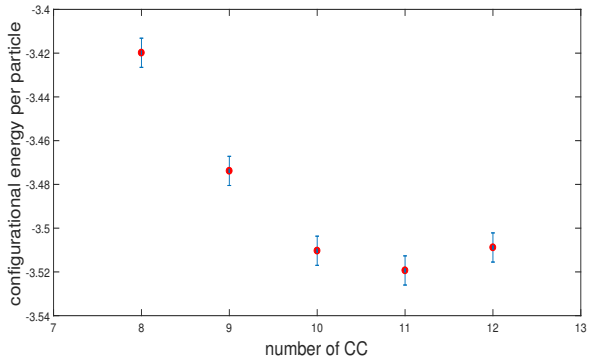

FIG. 5. The corresponding average configurational energy per particle of simulations in Figure 4 (error bars at 1σ).

Figure 6 shows the final configurations for simulations initiated with composite clusters of various sizes. Each simulation consists of 4000 particles of each component and a cubic simulation box with period boundaries with side length 55, giving the required overall system density, as before, very close to 0.024 for each component. Each simulation includes exactly 12 clusters of each component, stitched together to form large composite clusters. An interesting issue arises for the largest composite clusters, in that they are longer than the side length of the simulation cell. In this case, to ensure they are not 'bent' and do not 'meet' themselves, and can therefore equilibrate properly, we take advantage of the periodic boundaries and initiate these clusters at an angle to the simulation cell.

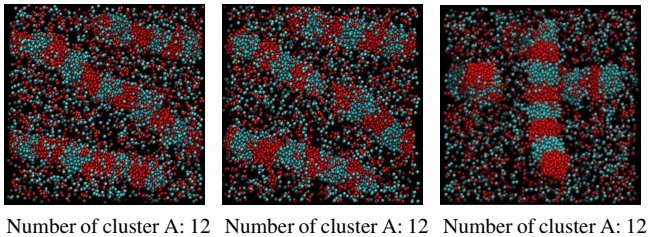

Number of cluster A: 12 Number of cluster B: 12 Number of CC: 1

Number of cluster A: 12 Number of cluster B: 12 Number of CC: 2

Number of cluster A: 12 Number of cluster B: 12 Number of CC: 3

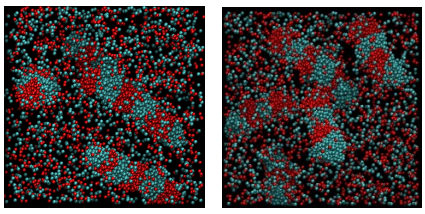

Number of cluster A: 12 Number of cluster B: 12 Number of CC: 4

Number of cluster A: 12 Number of cluster B: 12 Number of CC: 6

FIG. 6. Final configurations for simulations initiated with different numbers of large composite clusters, but the same total number of clusters when $A_{aAB} = 0.7, A_{rAB} = 0.1$.

Figure 7 shows the average energy for these simulations. We see that the lowest energy corresponds to the case with a single, very long composite cluster. Essentially, this simulation consists of parallel rows of fused, alternating clusters of relatively pure A and B. We interpret this to mean that for this combination of cross parameters and overall system density the equilibrium configuration no longer corresponds to a dispersion of isolated clusters, i.e. we are no longer within the cluster fluid phase. Instead, it appears that we have entered a more ordered region of the phase diagram consisting of columns of particles, in this case with alternating regions of type A and B. This is expected based on earlier work by Archer and Wilding[27], for example, that shows more ordered, modulated, configurations are expected for pure SALR fluids at higher overall system concentrations, or equivalently, for stronger interactions at the same overall concentration.

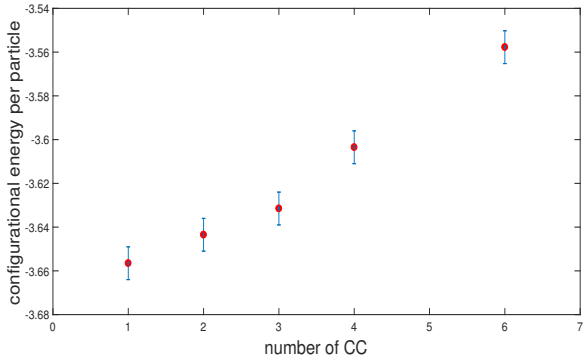

FIG. 7. The average configurational energy per particle of simulations in Figure 6(error bars at 1σ).

It follows that we can expect to re-enter the cluster fluid phase consisting of a uniform dispersion of equilibrium clusters, each of which is expected to consist of a pair of clusters of type A and B stuck together, by slightly reducing the strength of the attractive contribution to the cross-interaction or by reducing the overall system concentration. To test this hypothesis, we reduced the cross-interaction strength from 0.7 to 0.6 and repeated our process to find the equilibrium state. Figure 8 compares the two cases, and it can clearly be seen that our expectation is borne out. The equilibrium case now corresponds to case 2, i.e. composite clusters composed of pairs of clusters of type A and B stuck together.

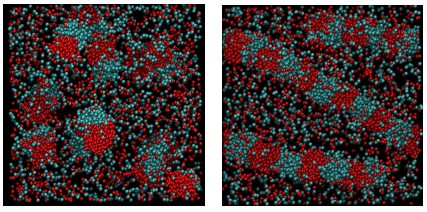

$A_{aAB} = 0.6, A_{rAB} = 0.1$ $A_{aAB} = 0.7, A_{rAB} = 0.1$

FIG. 8. Final snapshots of two simulations with different cross-attraction strengths

One may notice that the above optimization method is not perfect because the individual cluster size and the composite cluster size might influence each other and we did not consider all possible configurations of composite clusters. However, an exhaustive search would be very laborious, and we do not expect it would alter our conclusion, which is that under the conditions for case 4 long chains of fused clusters are expected.

B. Radial distribution functions

We now return to the simulations shown in Figure 3 to investigate pair correlations in these SALR fluids for cases representative of situation 1, 2 and 3. However, rather than simply plotting the particle-particle radial distribution function (rdf), denoted $g(r)$, we instead focus on a modified function which eliminates the contribution from pair correlations in the background vapour which are of little interest to us. Therefore, in this paper, we use the following partial rdf, denoted $g_p(r)$, for which only particles considered to reside within clusters are counted. In this work, particles are considered to reside within clusters if they have at least 9 neighboring particles within a range of 1.5. The partial rdf is evaluated separately at each sampling point, and then averaged at the end of a simulation. Using this partial rdf it becomes easier to see the contribution of cluster degrees of freedom.

Figures 9 and 10 show $g_p(r)$ corresponding to cases 1, 4 and 7, with A-A correlations displayed in Figure 9 and A-B correlations displayed in Figure 10. In Figure 9, the three A-A plots look somewhat similar to those for the pure SALR fluid with giant clusters simulated by Sweatman et al. using a similar pair interaction. However, there are some clear differences between the different cases. Most obviously, for case 1 corresponding to situation 1 (dispersed relatively pure clusters), we see a large dip in pair correlations at intermediate range, indicating that clusters of the same type almost never meet. This shows why these simulations are considered metastable states, because cluster splitting or combining events almost never occur. At short range we see that cases 1 and 4 corresponding to situations 1 and 2 (relatively pure dispersed clusters and composite clusters respectively) have very similar pair correlations, while the pair correlations for case 7 (situation 3, mixed clusters) are somewhat reduced, as expected. We also see that pair correlations are somewhat longer-ranged for case 7 because these mixed clusters are larger.

For case 4 (situation 2) we observe a decaying oscillatory trend, indicative of the long, fused clusters in this simulation. Case 7 (situation 3) shows behavior similar to case 1 at long range, which is expected because they both involve dispersed clusters. But there is a significant difference at intermediate range, in that we see a much greater tendency for the mixed clusters to approach each other closely. This reflects the subtle balance between short-range attraction and long-range repulsion in the mixed cluster state.

Looking now at Figure 10 for A-B pair correlations, we see immediately that for case 1 (situation 1) the clusters are relatively pure, since A-B correlations are very low within clusters in this state. We also see at short range that the strength of pair correlations is reversed compared to A-A correlations in Figure 9 for cases 4 and 7 (situations 2 and 3). This is expected because case 7 consists of mixed clusters. We continue to see the oscillatory decaying nature of pair correlations for case 4 (situation 2), although the phase is shifted compared to A-A pair correlations, as expected.

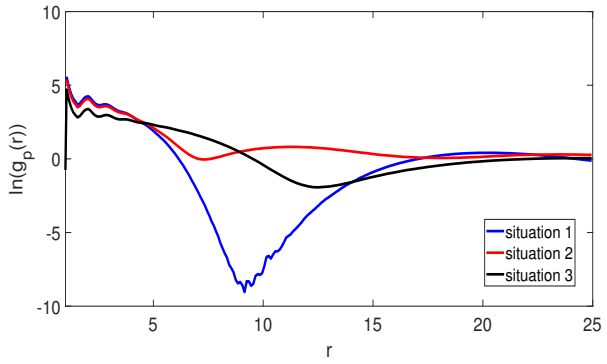

FIG. 9. The A-A partial radial distribution function for case 1 ($A_{aAB} = 0.35$ and $A_{rAB} = 0.1$), case 4 ($A_{aAB} = 0.7$ and $A_{rAB} = 0.1$) and case 7 ($A_{aAB} = 1.05$ and $A_{rAB} = 0.1$), corresponding to situations 1, 2 and 3 respectively.

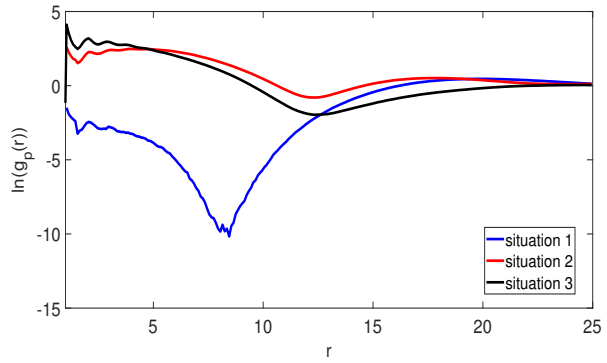

FIG. 10. As for Figure 9, except the A-B partial radial distribution function is plotted instead.

IV. CONCLUSIONS

We used Monte Carlo simulation to understand clustering behavior in symmetric SALR binary mixtures at low concentration, focusing on the cluster fluid state. We found that behavior can be tuned by adjusting the balance between short-range cross attractions and long-range cross repulsions. Specifically, for SALR systems that would form an equilibrium cluster fluid for each pure component separately, we find that when short-range cross-attractions dominate a dispersion of mixed clusters can occur (situation 3). This situation has previously been used to model WASP clusters, a form of membraneless organelle, adsorbed at cell membranes[23]. As

the short-range cross-attraction is gradually weakened, or as the long-range cross-repulsion is strengthened, we find these mixed clusters separate to form composite or fused clusters of slightly smaller relatively pure individual clusters (situation 2). Weakening the cross-attraction, or strengthening the cross-repulsion, further leads to a dispersion of individual relatively pure clusters (situation 1).

Although our simulations are necessarily limited in scope due to the large number of degrees of freedom in the model SALR potentials, we do not expect to see other cluster fluid states due to symmetry considerations. But we do have some further observations on this behavior. First, we expect the changes between these states (called 'situations' above) to occur gradually as the pair potential parameters are varied. These are not expected to be phase transitions. For example, the transition from situation 3 (mixed clusters) to situation 2 (relatively pure fused clusters) will likely involve the growth of domains of relatively pure A and B within each mixed cluster. Likewise, the transition from situation 2 to situation 1 (dispersed relatively pure clusters) will likely involve the gradual detachment of the clusters. Taking this to its logical extreme, when long-range cross repulsions dominate, we can expect a cluster solid (either a disordered Wigner glass or an ordered crystal) of alternating cluster types to occur. We did not simulate this case because it is no longer a cluster fluid state. The details of these gradual changes can be investigated in future work.

Secondly, we expect that, just as for the pure SALR fluid, as system concentration increases, the full range of ordered, or modulated, cluster states will occur until a bulk SALR liquid is formed at high concentrations. We already saw for case 4 that long chains of fused clusters occurred under the conditions simulated, and we argued that at lower concentrations we should observe a cluster fluid state consisting of pairs of fused clusters (situation 2). We observed this state by reducing the strength of cross-attractions slightly. Future work can also investigate the details of these cluster states at higher concentrations.

Thirdly, we have chosen SALR parameters similar to earlier work for the pure component case and to ensure individual clusters are not too large, and therefore not too expensive to simulate. However, it is clear that, just as for the single component case, clusters with a wide range of sizes can be designed by adjusting the balance between short-range attractions and long-range repulsions in both the direct and cross-interactions. One way of tuning cluster size might be to adjust the temperature, because temperature will likely influence the strength of short-range attractions and long-range repulsions in different ways. This is because these are effective interactions resulting from different physical processes. However, adjusting this balance, by adjusting the temperature for example, might also have other consequences. For example, altering the balance between short-range cross-attractions and long-range cross-repulsions might also cause the system to switch between the different kinds of basic behavior observed in this work, e.g. from a mixed cluster state (situation 3) to a fused cluster state (situation 2).

These observations could have important consequences for any solute system that can be modelled approximately in terms of a symmetric binary SALR interaction, for example polyelectrolytes designed to form self-assembling templates for novel nanomaterials. In this case, the ability to control the type of templating cluster formed affords control over the final engineered nanomaterial. We show that it should be possible to simultaneously form clusters with different compositions, provided the long-range cross-repulsion dominates the cross interaction. These relatively pure clusters can be encouraged to fuse to form composite clusters by increasing the strength of the short-range cross-attraction slightly, which extends the possibilities for templated materials much further. For example, templated nanospheres with an opening on one side might be formed if the templated material is attracted to only one of the solutes. Alternatively, at higher solute concentrations, long tubules of alternating materials might be formed. But increasing the attractive cross-interaction too much would produce mixed clusters instead.

DATA AVAILABILITY

The data that supports the findings of this study are available within the article.

[1] A. Stradner et al., *Nature* **432**, 492 (2004).
[2] D. Gebauer, A. Völkel, and H. Cölfen, *Science* **322** , 1819 (2008).
[3] A. Jawor-Baczynska, J. Sefcik, and B. D. Moore, *Crystal growth and design* **13** , 470 (2013).
[4] S. Chattopadhyay et al., *Crystal growth and design* **5** , 523 (2005).
[5] X. Zhang, H. Sun, and S. Yang, *The Journal of Physical Chemistry C* **116** , 19018 (2012).
[6] M. Li, H. Schnablegger, and S. Mann, *Nature* **402** , 393 (1999).
[7] Bernabei. Marco et al., *Soft Matter* **9** , 4 (2013).
[8] Slimani. Mohammed Zakaria et al., *ACS macro letters* **3** , 7 (2014).
[9] Buttinoni, Ivo et al., *Physical review letters* **110** , 23 (2013).
[10] Mani, Ethayaraja and Löwen, Hartmut, *Physical Review E* **92** , 3 (2015).
[11] Y. M. Ramdzan et al., *Nature methods* **9** , 467 (2012).
[12] A. Centi et al., *Materials Horizons* **6** , 1027 (2019).
[13] Jadrich. Ryan B et al., *Soft Matter* **11** , 48 (2015).
[14] Lindquist, Beth A et al., *Soft Matter* **13** , 7 (2017).
[15] Foffi. G et al., *The Journal of chemical physics* **122** , 22 (2005).
[16] Klix. Christian L and Royall. C Patrick and Tanaka. Hajime, *Physical review letters* **104** , 16 (2010).
[17] Van Schooneveld et al., *The Journal of Physical Chemistry B* **113** , 14 (2009).
[18] Zhang. Tian Hui et al., *Soft Matter* **8** , 3 (2012).
[19] Zaccarelli, Emanuela, *Journal of Physics: Condensed Matter* **19** , 32 (2007).
[20] Ruzicka. Barbara and Zaccarelli. Emanuela *Soft Matter* **7** , 4 (2011).
[21] M. B. Sweatman, R. Fartaria, and L. Lue, *The Journal of Chemical Physics* **140** , 124508 (2014).
[22] M. B. Sweatman, and L. Lue, *Advanced Theory and Simulations* **2** , 1900025 (2019).
[23] M. B. Sweatman, and R. Insall, *Advanced Theory and Simulations* **2** , 1800203 (2019).
[24] M. B. Sweatman, and L. Lue, *The Journal of Chemical Physics* **144** , 171102 (2016).
[25] M. B. Sweatman *Molecular Physics* **116** , 1945 (2018).
[26] A. J. Archer, *Physical Review E* **78** , 031402 (2008).
[27] A. J. Archer, and N. B. Wilding, *Physical Review E* **76** , 031501 (2007).
[28] Godfrin P D, et al. *Soft Matter* **10** , 28 (2014).
[29] Bomont, Jean-Marc and Costa, Dino and Bretonnet, Jean-Louis *Physical Chemistry Chemical Physics* **19** , 23 (2017).
[30] Bollinger, Jonathan A and Truskett, Thomas M *The Journal of Chemical Physics* **145** , 6 (2016).

[31] Archer A J, et al *Journal of Physics: Condensed Matter* **20** , 41 (2008).
[32] Archer, A J and Evans, R *Molecular Physics* **109** , 23-24 (2011).
[33] Bomont J M, Costa D, Bretonnet J L *Physical Chemistry Chemical Physics* **22** , 9 (2020).
[34] Bomont J M, Costa D, Bretonnet J L *AIMS Materials Science* **7** , 2 (2020).
[35] Bomont J M, et al *The Journal of Chemical Physics* **137** , 011101 (2012).
[36] C. A. Ferreiro-Rangel, and M. B. Sweatman *Molecular Physics* **116** , 3231 (2018).
[37] W. Humphrey, A. Dalke, and K. Schulten, *Journal of molecular graphics* **14** , 33 (1996).